Biomechanics of the peafowl's crest reveals frequencies tuned to social displays

Suzanne Amador Kane*[1], Daniel Van Beveren[1], Roslyn Dakin[2,3]

[1] Physics Department, Haverford College, Haverford, PA 19041, USA
[2] Department of Zoology, University of British Columbia, Vancouver, BC V6T1Z4, Canada
[3] Migratory Bird Center, Smithsonian Conservation Biology Institute, P.O. Box 37012, Washington, DC 20013, USA

*corresponding author: samador@haverford.edu

Short title: Biomechanics of peafowl feather crests

Keywords: feather; mechanoreception; resonance; near-field sensing; peacock; multi-modal signaling

ABSTRACT

Feathers act as vibrotactile sensors that can detect mechanical stimuli during avian flight and tactile navigation, suggesting that they may also detect stimuli during social displays. In this study, we present the first measurements of the biomechanical properties of the feather crests found on the heads of birds, with an emphasis on those from the Indian peafowl (*Pavo cristatus*). We show that in peafowl these crest feathers are coupled to filoplumes, small feathers known to function as mechanosensors. We also determined that airborne stimuli with the frequencies used during peafowl courtship and social displays couple efficiently via resonance to the vibrational response of their feather crests. Specifically, vibrational measurements showed that although different types of feathers have a wide range of fundamental resonant frequencies, peafowl crests are driven near-optimally by the shaking frequencies used by peacocks performing train-rattling displays. Peafowl crests were also driven to vibrate near resonance when we played back mechanical sounds generated by these displays in the acoustic very near-field, where such displays are experienced *in vivo*. When peacock wing-shaking courtship behaviour was simulated in the laboratory, the resulting airflow excited measurable vibrations of crest feathers. These results demonstrate that peafowl crests have mechanical properties that allow them to respond to airborne stimuli at the frequencies typical of this species' social displays. This suggests a new hypothesis that mechanosensory stimuli could complement acoustic and visual perception of social displays in peafowl and other bird species. We suggest behavioral studies to explore these ideas and their functional implications.

INTRODUCTION

Bird feathers are known to be coupled to vibration-sensitive nerve endings at their bases that can allow birds to sense and respond to a variety of mechanical stimuli (Saxod, 1978; Necker, 1985b; Brown and Fedde, 1993). For example, flight, contour, and facial bristle feathers can act as sensors that provide important information during flight (Bilo and Bilo, 1978; Brown and Fedde, 1993; Brücker et al., 2016) and prey capture (Cunningham et al., 2011), and birds change their posture in response to air flows directed at their heads (Bilo and Bilo, 1983). Indeed, because even isolated protofeathers could have played a sensory role early in evolution, feathers have been suggested to have evolved originally to serve sensory functions, given that thermal regulation and flight both require dense coverings of specialized plumage (Persons and Currie, 2015). More recently, behavioral studies of two auklet species have shown that their erect head crest feathers also play a mechanosensory role during tactile navigation similar to that of mammalian whiskers and arthropod antennae (Seneviratne and Jones, 2008; Seneviratne and Jones, 2010). Feather crests are found on the heads of a wide variety of bird species, as well as on some dinosaur and early bird fossils (Lindow and Dyke, 2006; Li et al., 2010). These findings suggest a new functional role for these feather ornaments, which have previously been studied for their roles as possible visual signals (Burley and Symanski, 1998; Jones and Montgomerie, 1992; Hagelin, 2002; see also Seneviratne and Jones, 2008 for a review), and calls for an exploration of how their biomechanical properties relate to their various proposed functions.

Here we report on the first biomechanical study of crest feathers, with an emphasis on the response of the crest of the Indian Peafowl (*Pavo cristatus*) to static, impulsive and oscillatory vibrational bending forces. This work was designed to serve as a first step in providing context for exploring whether the head crests of birds might serve a variety of mechanosensory functions, including the detecting body self-motion and various airborne stimuli. We used our data to determine whether peafowl crests are frequency-matched to the motions used by these birds during body-shaking social displays. To probe how crest vibrational responses vary among other birds, we also compared the properties of peafowl crest feathers to crest feathers from five other species.

Other animals are known to detect acoustic particle velocity oscillations in a variety of ways, including using sensory hairs and antennae that resemble feathers (Fletcher, 1992; Larsen and Wahlberg, 2017). For example, just as sensory hairs and antennae have mechanosensors at their bases, feathers of all types (including head, flight and contour) in birds of all orders are associated at their bases with specialized mechanosensitive feathers called filoplumes that couple to the longer feather's shaft and function as bend and vibration detectors (Lucas and Stettenheim, 1972; Weir and Lunam, 2011). Both contour feathers and filoplumes have been shown empirically to detect bending and vibrations via Herbst corpuscles, a type of bending- and vibration-sensitive mechanoreceptor situated at their bases (Necker, 1985a; Necker, 1985b; Brown and Fedde, 1993; Stettenheim, 2000). As is the case for many arthropod sensory hairs, the plumose structure of feathers also enables effective coupling to air motions via drag forces that can bend the feather shaft and stimulate mechanoreceptors at its base (Necker, 1985b; Bradbury and Vehrencamp, 2011). Like many sensory hairs and antennae, bird feather shafts (rachises) also consist of an elongated, tapering cylinder with a rigid outer cortex and shock-absorbing core that can bend so as to transmit forces to its enervated base. A large body of research in mammals and arthropods has found that antennae and sensory hairs play important mechanosensory roles in sound detection that are directly related to their vibrational response and mechanical structures (Barth et al., 2012; Sofroniew and Svoboda, 2015). However, no research has considered whether birds might use both their ears and non-auditory senses to detect similar air-borne signals during social displays, or what influence this may have on their social interactions.

In one notable example of such a multimodal display, male Indian peafowl ("peacocks") attract mates by spreading, erecting and vibrating their train, a fan-like array of long, colorful feathers, and by shaking their wings (Fig. 1A, Movie S1). First, in the wing-shaking display, the peacock orients his backside toward nearby females ("peahens") and flaps his partially unfurled wings at approximately 5.4 Hz. Second, in the train-rattling display, the peacock faces a female at close range (approximately 1 to 1.5 m) and shakes his tail and train feathers rapidly at 22-28 Hz (mean = 25.6 Hz), causing his train to shimmer iridescently and emit a prolonged "rattling" sound (Dakin and Montgomerie, 2009; Freeman and Hare, 2015; Dakin et al., 2016). Train-rattling performance by peacocks is obligatory for mating success (Dakin and Montgomerie, 2009), and

eye-tracking experiments have shown that both wing-shaking and train-rattling displays are effective at attracting and holding the peahen's gaze (Yorzinski et al., 2013). Peahens also perform a tail-rattling display at 25-29 Hz in a variety of contexts (Dakin et al., 2016), suggesting that feather vibrations might serve other communicative functions as well.

Several behavioral studies have reported results consistent with birds being able to hear and respond to similar low frequency sounds. Behavioral studies have measured the auditory response of other bird species to amplitude-modulated low repetition rate broad-band pulses, which are similar to the mechanical sounds associated with peacock train-rattling; the results of these studies showed that birds from three different families can hear sounds with repetition rates < 40 Hz (Dooling and Searcy, 1981; Klump and Okanoya, 1991; Dent et al., 2002). Three more recent studies have also reported behavioral responses of birds to playbacks of low frequency sound by distant speakers: e.g., indicating that peafowl detect the infrasound (< 20 Hz) component of train-rattling and wing-shaking recordings (Freeman and Hare, 2015), that male houbara bustards (*Chlamydotis undulata undulata*) respond to low frequency (40-54 Hz) boom vocalizations (Cornec et al., 2017), and that male ruffed grouse (*Bonasa umbellus*) respond to 45 ± 6 Hz wing beating "drumming" displays (O'Neil et al., 2018). By contrast, no studies have considered whether peafowl or other birds might detect mechanical sound via vibrotactile sensing.

In other animals, vibrotactile sensors detect sound particle velocity oscillations in the acoustic near-field, a region close enough to the source that particle velocity can couple efficiently to mechanoreceptors via drag forces (Fletcher, 1992). Near-field communication has been studied in a wide variety of invertebrate terrestrial taxa (Markl, 1983; Greenfield, 2002) and in fish (Sisneros, 2015). For example, in arthropods, many species use filiform hairs to detect near-field particle velocity for predator or prey detection and for intraspecies signaling (Greenfield, 2002; Santer and Hebets, 2008; Barth, 2014). However, such a mechanism for sound reception has not yet been considered in birds.

One possible means by which peafowl might sense near-field sound is the fan-like crest (Fig. 1A,B), a planar array of feathers oriented in the sagittal plane that is found on the heads of both

sexes (Dakin, 2011). Each crest feather has a spatulate, iridescent "flag" of pennaceous vanes at the distal end and a long shaft that is mostly bare except for short, sparse barbs along its proximal end (Fig. 1C). The pennaceous flag of peafowl crest feathers can couple to oscillations in surrounding air via drag forces induced by flow of the surrounding medium, as well as via forces exerted on the flag's face by incident pressure waves. Because the peafowl's region of most acute vision is oriented laterally (Hart, 2002), when a peahen gazes at a displaying male, the maximum area of her crest feathers also points toward the peacock's moving feathers (Fig. 1A). This results in an optimal orientation for intercepting airborne vibrations generated by display behaviors; these medium oscillations should tend to drive feather crests to oscillate in the "out-of-plane" orientation (i.e., normal to the plane of the crest as shown in Fig. 1D). Because the displaying bird shakes its body laterally during such behaviors, this also should drive its own feather crest to vibrate in the out-of-plane direction. The design of the crest also provides mechanical advantage, enabling it to transmit a magnified version of the forces applied to its distal end to its base, because the flag is wider than the tapered base and because each feather shaft acts as a lever arm coupling the flag to the base.

In this study, we investigated the biomechanical properties of avian crests to enable a comparison between their resonant properties and oscillatory airborne stimuli characteristic of social displays. While a significant body of literature exists on the mechanical properties of wing, tail and train covert feathers for a wide variety of bird species (Sullivan et al., 2017), no previous work has considered crest feathers or other types of feathers found on the head. To explore this question, we first review the physical acoustics relevant to vibrotactile detection of mechanical sounds. The reader may consult in-depth treatments for more details (Kalmijn, 1988; Blackstock, 2000; Fahy, 2001; Larsen and Wahlberg, 2017).

First, we consider how different sound source geometries determine how the acoustic far- and near-fields depend on sound wavelength, λ, source distance, R, and source size, A (Fletcher, 1992; Blackstock, 2000). The geometries relevant to this study include monopoles, which provide a model for loudspeakers, versus dipoles and vibrating circular disks, which provide a model for moving wings, tails and trains. The most familiar regime for sound reception is the acoustic far-field, which predominantly consists of pressure waves detectable by vertebrate ears,

insect tympanal organs and similar receptors. Because the particle velocity magnitude falls off more rapidly with distance than the pressure wave component, particle velocity stimuli are greater than those due to pressure waves only for distances $R < 0.16\ \lambda$ to $0.22\ \lambda$ for monopole and dipole sources, respectively (Kalmijn, 1988). Consequently, this wavelength-dependent distance is often used to distinguish the acoustic far- and near-fields. However, the relevant criterion for efficient mechanosensation is the *absolute magnitude* of particle velocity, not the *relative value* of particle velocity compared to the pressure wave (Rogers and Cox, 1988). Thus, the regime relevant for vibrotactile sensing is the flow (reactive) near-field: the region near the sound source where the particle velocity has its greatest magnitude because the air acts as a layer of effectively incompressible fluid that moves with the source (De Bree et al., 2004; Larsen and Wahlberg, 2017). The extent of the flow near-field depends on source size, A, not wavelength (see e.g., Fig. 2 in (De Bree et al., 2004)). For $R \leq 0.16\ A$ (the "very near-field"), the particle velocity is approximately constant. As R increases, particle velocity becomes negligible for mechanosensing at approximately $R \approx A$ (Fletcher, 1992; De Bree et al., 2004; Bradbury and Vehrencamp, 2011). The lateral extent of the flow near-field also depends on A. In addition, the overall magnitude of the particle velocity increases as A^2 for a monopole and A^3 for a dipole. In summary, increasing source size, A, increases the spatial extent of the flow near-field regime in which mechanoreception can take place, as well as the magnitude of particle velocity stimuli (Kalmijn, 1988).

From this background, we can infer that during the peacock's display, when typical female-male distances are equal to the typical peacock train radius, females therefore receive train-rattling sound in the flow near-field (Dakin and Montgomerie, 2009; Dakin and Montgomerie, 2011). Note also that because the criterion $R < 0.22\ \lambda$ holds for frequencies < 50 to 75 Hz at this distance, most of the human audible range components of the peacock's display also have appreciable pressure wave magnitude. Spectrograms from earlier studies of peacock train-rattling indicate that these mechanical sounds consist of broadband impulsive rattles with spectral density primarily in the human audible range, emitted at a repetition rate of approximately 26 Hz; they are neither low frequency pure tones, nor are they sound with spectral density predominantly in the low frequency or infrasound regime (Freeman and Hare, 2015; Dakin et al., 2016). As a result, a consideration of the sound fields of peacock train-rattling

displays indicates that rattling sounds might be detectable as particle velocity or pressure wave stimuli, or both, at typical display distances. Another consequence of the broadband nature of train-rattling is that rapid intensity variations due to interference at small R (the "interference near-field") should not be relevant for this display, because this effect depends on the superposition of sound waves with a well-defined frequency emitted by different parts of an extended source.

In this study, we explore the biomechanics of the peafowl crest, taking the first steps toward characterizing how its structure and mechanical properties might influence its possible functions. To do so, we first consider which features we would expect these feathers to have to function effectively as mechanosensors for different stimuli. For example, in order for the crest to sense environmental airflows, it would need to bend sufficiently to activate mechanosensory nerve cells, as has been shown for pigeon covert feathers (Necker, 1985b), arthropod sensory hairs, pinniped whiskers, bat sensory hairs, and fish lateral line organs (Bleckmann et al., 2014) and rat whiskers (Yu et al., 2016; Yu et al., 2016).

Frequency-tuning between stimuli and sensory structures can provide several advantages (Fletcher, 1992). For example, feather crests optimized to vibrate at the shaking frequency could provide proprioceptive feedback to the individual performing the display (Kämper and Dambach, 1981; Dambach et al., 1983; Fletcher, 1992). The crest also might detect airborne stimuli generated by a conspecific individual's shaking motions by undergoing sympathetic vibrations (i.e., undergoing oscillations driven by coupling through drag forces to air particle velocity oscillations). Such mechanical frequency tuning between the emitted and received sounds can be accomplished readily via resonance, the phenomenon whereby an object responds with maximum amplitude to a driving force that oscillates near one of its natural frequencies of vibration (Fletcher, 1992). Frequency-matching between the source and receiver response is known to occur in a variety of arthropods, such as arachnids that use their trichobotheria to sense prey wingbeats, various species of insect that use their antennae to detect wingbeat signals of near-by conspecifics (e.g., insects that use their sensory hairs to sense wingbeats of predatory wasps (Tautz and Markl, 1978; Kirchner, 1994; Magal et al., 2006; Tsujiuchi et al., 2007; Barth, 2013) and cicadas and crickets that use frequency-tuned eardrums to detect conspecific songs in

the far-field (Paton et al., 1977; Sueur et al., 2010)). Given that peafowl displays also take place at well-defined shaking frequencies, if feather crests have a resonant frequency response with a peak and width matched to the display, they could respond with optimal sensitivity to low amplitude airborne stimuli associated with displays while filtering out background noise and other irrelevant stimuli, at the expense of frequency discrimination. This is indeed the case for the arthropods cited above. (Note that this is in contrast to the operation of human eardrums and microphones, which have broadly-tuned resonance responses that allow efficient detection of natural stimuli over a wide range of frequencies.)

Another possible function found in some arthropods is the ability to use mechanoreception to sense separate airflow pulses generated by abrupt, repetitive motions similar to peacock wing-shaking. The resulting impulsive forces result in the hairs undergoing oscillations at their natural frequency that are damped out in the intervals separating each distinct pulse. For example, the cerci sensory hairs of female African crickets (*Phaeophilacris spectrum*) function in this way to detect air vortices produced by males performing wing flicks (Heinzel and Dambach, 1987; Heidelbach and Dambach, 1997; Lunichkin et al., 2016). Detecting airflow impulses via transient oscillations requires the right combination of damping and resonant frequency to allow a high amplitude response while also enabling detection of the airflow impulse repetition rate.

We measured the vibrational response of intact and individual peafowl crest feathers, along with the response of peafowl crest feathers to static and impulsive bending forces and audio playbacks of peacock train-rattling. We used high-speed video to measure the resonant frequencies of peafowl feather crests and individual crest feathers and how sharply tuned such resonances are, and compared those values with *in vivo* train- and tail-rattling shaking frequencies (Dakin et al., 2016). Similar video and imaging-based methods have been used to measure resonance in whiskers (Hartmann et al., 2003; Wolfe et al., 2008; Shatz and Groot, 2013; Hans et al., 2014), insect antennae (Dirks and Dürr, 2011), feathers (Gao et al., 2015) and human-made structures (Ferrer et al., 2013; Paunescu et al., 2015). Because interactions between feathers can influence their resonant frequency and damping (Cummins and Gedeon, 2012), we compared the biomechanics of whole crests to that of isolated crest feathers. To test whether mechanical sound might cause crest motion in females located in the near-field of train-rattling peacocks, we also

measured deflections of crests that were exposed to audio playbacks of train-rattling and a white noise control.

We also wished to determine whether any agreement between social display frequencies and crest resonant frequencies was generic or specific to this system. Therefore, we sought to understand how the peafowl crest's resonant properties relate to those of other feathers from peafowl and other species. The crest feathers of different birds have a variety of orientations, morphologies and erectile properties. For example, cockatoos (family *Cacatuidae*), Victoria crowned pigeons *Goura victoria*, and hoopoes *Upopa epops*, all have very long crests, whereas the double-crested cormorant, *Phalacrocorax auritus*, and tufted titmouse, *Baeolophus bicolor*, have very short crest feathers. Consequently, we also measured the resonant response of crest feathers from four other bird species to vibrational oscillations to evaluate how these properties vary between species.

Motivated by reports that mechanosensitive auklet crests feathers are filoplumes (Seneviratne and Jones, 2008) and the proposal that protruding filoplumes found on the heads of birds from diverse species spanning several orders might function to detect disturbances of the surrounding feathers (Imber, 1971; James, 1986; Childress and Bennun, 2002; Clark and de Cruz, 1989), we also used microscopy to determine the relationship between peafowl crest feathers and filoplumes.

Finally, we considered the peacock's wing-shaking display. We tested whether the wing-shaking display resulted in periodic airflow disturbances that could drive transient crest feather vibrations. To do so, we used high-speed video to visualize the responses of peafowl crests to airflow produced by a wing-flapping robot during simulated wing-shaking displays. Because the wing-shaking display is expected to generate periodic airflow impulses at a lower frequency as compared to train-rattling (about 5 Hz for wing shaking vs. 26 Hz for train-rattling), we also conducted an experiment to determine how peafowl crests respond to individual airflow impulses.

MATERIALS AND METHODS

In vitro samples

A total of n = 7 male and n = 8 female Indian peafowl (*Pavo cristatus* Linnaeus 1758) head crests with the feathers still mounted in skin were purchased from commercial vendors. We obtained other types of peacock feathers and crest feathers from three other bird species from zoos and aviaries (see Table S1 and Fig. S1 for details). A Digital Microscope Pro (Celestron, Torrance, CA USA) was used to examine the base of peafowl crest feathers to determine whether filoplumes were present, using the structural criteria employed in previous studies of this feather type (i.e., short feathers with a long, bare shaft with a tuft of short barbs on the distal end, located near the base of a longer feather but not growing from the same follicle (Imber, 1971; Lucas and Stettenheim, 1972; James, 1986; Clark and de Cruz, 1989; Childress and Bennun, 2002; Williams et al., 2015); see micrographs in (Lucas and Stettenheim, 1972; Necker, 1985a; Williams et al., 2015). Crest length and width measurements were made by hand and from digital photographs of the crest samples and high-resolution scans (0.02 mm/pixel) of single feathers with a ruler included in the sample plane. We used these measurements to compare the morphology of dried crest samples with that of crests on live peafowl in a previous study (Dakin, 2011), including length, width and number of feathers. Because some peafowl, especially females, have non-uniform crest feather lengths (Dakin, 2011), we also measured the lengths of individual feathers within the dried crest samples to compare with the previous study.

For mechanical testing, we glued the lower side of the crest skin to a rigid sample holder (a 2.5 cm cube of balsa wood) using hot glue (Fig. 1D). An earlier study comparing the resonance of feathers mounted using rigid balsa wood versus a compliant gel found that the compliant mounts resulted in only slightly lower resonant frequencies and reduced amplitudes at frequencies > 50 Hz (Dakin et al., 2016), as expected for a flexible shaft secured by a stiff clamp (Fletcher, 1992). If the crest feathers were closely clustered, the attached skin was first softened in water and the crest was spread to approximate its natural configuration. To study individual, isolated crest feathers, we removed all but three to five feathers (on the outer edges and in the middle) from two male crests and one female crest and analyzed the characteristics of those remaining feathers. Note that because this procedure was necessarily destructive, it precluded any further whole-crest analyses on those samples, so we limited it to only the three crests. Isolated body

and crest feathers were inserted into a close-fitting hole in the wood base using polyvinyl acetate glue. For measurements on other peafowl feathers and crest feathers from other species, all but two feather samples in Table S1 were inserted up to the top of their calamus (the part of the shaft inserted into the skin). The Victoria crowned pigeon crest feathers had been trimmed just above the calamus, so they were mounted such that 3 mm of the exposed feather shaft (3% of its length) was inserted into the wooden base.

Because earlier research on feather keratin indicated that water content can affect its elastic modulus (Taylor et al., 2004), all crest samples were stored and all laboratory measurements were taken at 21.1 C^{o} (range: 20.8-21.5^{o}) and 74.8% relative humidity (range 72.3-77.7%). For comparison, peacock train-rattling display frequencies were measured in the field at a median temperature of 19.4ºC and a median relative humidity of 60.7% (Dakin et al., 2016), with over half of the displays occurring within ±2.2ºC and ±14% of the average laboratory temperature and relative humidity, respectively. Moreover, a re-analysis of previous published data on 35 peacock displays performed by 12 males in the field (Dakin et al., 2016) shows that there is no significant association between display vibration frequency and relative humidity ($p > 0.45$) when accounting for the date and time of the displays. This analysis and the associated data are provided in the data repository for this study (Dakin et al., 2018). As an additional check, we also measured the audio playback response with crest samples held at 35% relative humidity and 22 C^{o} for 1 min to 10 min and found no measurable change in the natural frequency over this time.

Vibrational dynamics measurements

There are two standard methods for determining a mechanical system's vibrational response: 1) Apply a sinusoidal driving force and amplitude to the sample while measuring its resulting vibrational amplitude as a function of the driving frequency. The vibrational response is then computed as the ratio of the sample's response to the driving stimulus magnitude (the transfer function) (Hartmann et al., 2003; Bostwick et al., 2009; Clark et al., 2013). 2) Apply either a step deflection or an impulsive force to provide a stimulus with a broad, uniform frequency spectrum, then measure the vibrational response of the sample as a function of time. If a single resonant mode of vibration is excited, then the sample's response corresponds to a sinusoid at the

natural frequency with exponentially decaying amplitude (Hartmann et al., 2003; Neimark et al., 2003; Wolfe et al., 2008; Dirks and Dürr, 2011; Gao et al., 2015). Below we describe how we performed each of these tests, as well as establishing the linearity of bending elasticity of the peafowl crests.

For vibrational dynamics measurements, the feather assembly was mounted on a model SF-9324 mechanical shaker (Pasco Scientific, Roseville, CA, USA) driven by an Agilent 33120A function generator (Agilent Technologies, Wilmington, DE, USA) (Fig. S1). Two orthogonal directions of the driving force were used: “out-of-plane”, oriented normal to the plane of the crest; and “in-plane”, oriented parallel to the plane of the crest and in the posterior-anterior axis of the head (Fig. 1D). The first orientation (out-of-plane) corresponds to the geometry when a peafowl either visually fixates the display by orienting one side of the head towards it, or else drives its own crest into vibrations by performing a train- or tail-rattling display (Dakin et al., 2016). The second (in-plane) orientation recreates the geometry when the front of the head is oriented towards the display or when the bird bobs its head during feeding or walking. The vibrational response spectrum was measured using three linear frequency sweeps, defined below, with rates of frequency increase chosen to be less than the values measured at the start of peafowl displays in an earlier study (Dakin et al., 2016). Each of the 15 crests was tested three separate times in the out-of-plane orientation at the 0-80 Hz frequency range (sweep rate 1.33 Hz/s; n = 45 trials). We also ran trials using the following sweep rates to make sure that changing the sweep rate did not reveal new spectral features at very low frequencies or between 80 and 120 Hz, or influence the measured value of resonant frequency: six crests out-of-plane at 10-120 Hz (1.83 Hz/s; n = 18 trials), six crests at 0-15 Hz (0.25 Hz/s, n = 6 trials), five crests in-plane at the 0-80 Hz range (1.33 Hz/s; n = 14 trials), and two crests in-plane at 10-120 Hz (1.83 Hz/s; n = 2 trials). Finally, we tested three crests out-of-plane after they had been trimmed down to have only three to five isolated crest feathers remaining (3 feathers for male Crest 03, 5 for male Crest 05 and 3 for female Crest 10), at 0-80 Hz (1.33 Hz/s; n = 9 trials), to evaluate the vibrational response of isolated crest feathers. For one crest, we also determined that varying the amplitude of shaking by a factor of four resulted in the same resonant response within measurement error.

We also measured the resonant response of crest feathers for several other types of short peacock feathers (three lengths of peacock mantle feathers, the shortest length of train eyespot feather, and four different body contour feathers), and for one or more crest feathers from four other bird species: two additional species from order Galliformes, the Himalayan monal (*Lophophorus impejanus*) and the golden pheasant (*Chrysolophus pictus*); the Victoria crowned pigeon (*Goura Victoria*) from the order Columbiformes, and the yellow-crested cockatoo (*Cacatua sulphurea*) from the order Psittaciformes; see Table S1 and Fig. S1 for details. The resonant response for each of these feathers was measured for driving forces in the out-of-plane direction for n = 3 trials for each feather at each of two frequency sweep rates (2.0 Hz/s, 0 to 120 Hz; 1.33 Hz/s, 0 to 80 Hz); the Himalayan monal sample was also studied using a sweep rate of 0.5 Hz/s over 0 to 30 Hz because it had a lower frequency response.

Video analysis

We recorded feather vibrational motions using high-speed video filmed with a GoPro Hero 4 Black Edition camera (720 x 1280 pixels; 240 frames s^{-1}; GoPro, San Mateo, CA, USA). Image and data analysis were performed using custom programs based on the MATLAB 2015a Machine Vision, Signal Processing and Curve Fitting toolboxes (MathWorks, Natick, MA, USA); the MATLAB scripts to reproduce this analysis are available with the data repository for this study (Dakin et al., 2018). Lens distortion was first removed using the MATLAB Camera Calibration tool. All feather motions analyzed were in the plane of the image, and thus did not require correction for perspective (Biewener and Full, 1992). To analyze feather motion, we first used auto-contrast enhancement and thresholding to track the mean position of the crest feather flags and the shaker mount, and then computed the spectrogram of each object's tracked position during the frequency sweep using a Hanning filter. This yielded the magnitude of the fast Fourier transform (FFT) at each vibrational drive frequency, f_d, measured for motion of the crest flag, A, and that of the sample holder, A_d, which provides the driving force. Mechanical shakers have a frequency response that necessarily rolls off in amplitude at the low frequencies considered here due to fundamental physical principles (Smith, 2010); see, e.g. inset to Fig. 1A in (Clark et al., 2017). To account for frequency-dependent variation in the driving force, we then divided the sample's magnitude, A, by the shaker drive magnitude, A_d, at that frequency to give the drive transfer function, (A/A_d) (Hartmann et al., 2003; Bostwick et al., 2009). Below,

we describe two further tests for the validity of this procedure: measurements of the natural frequency using the impulse method and direct measurement of the linearity of the bending elastic response. The Nyquist frequency, which gives the upper bound on measurable frequencies (Smith, 2010), was 120 Hz (half the frame capture rate) (> 4X typical biological vibration frequencies used during peafowl displays). Finally, the drive transfer function was smoothed over a 1.3 Hz window using a cubic Savitzky-Golay filter and all peaks in the response were fit to a Lorentzian function using nonlinear-least squares fitting to obtain the resonant frequency, f_r, and full-width-half-maximum, Δf, of the spectral power (Smith, 2010). These fits were performed in Origin 8.6 (Originlab, Northhampton, MA, USA). The quality factor, Q (a measure of how sharply defined the resonant frequency is), was computed from $Q = f_r/\Delta f$.

Force impulse experiments

To determine the crest's response to impulsive airflows, we applied single air ring vortices to the crests and measured the resulting motions on video. A Zero Blaster vortex gun (Zero Toys, Concord, MA, USA) was used to generate single air vortex rings of artificial fog (2-4 cm in diameter, 1 cm diameter cross-section, speed 1.8 m/s [95% CI 1.7, 2.0 m/s, range 1.5 - 2.1 m/s]), aimed so as to impact whole crests (n = 2 peacock and 1 peahen) in the out-of-plane orientation. The motion of crest feathers struck by the vortices was measured by tracking the crest position on high-speed video when an intact vortex impacted the crest oriented with its widest cross-section facing the source at 0.5 m from the point of creation. As explained above, because we expected such impulses to result in the crest feathers oscillating at their natural frequency, this provided an additional check on our resonant frequency values. This also provides a model for understanding how crest feathers would respond to impulsive airflows generated by other sources (e.g., displays, wind, etc.)

Audio playback experiments and analysis

To determine if peafowl crests can vibrate detectably due to peacock train-rattling, we filmed high-speed video of peahen crest samples placed in the flow near-field of a loudspeaker playing back train-rattling sounds. Note that because peacock train-rattling consists of broad-band rattles at low repetition rates, not pure tones, we used audio equipment rated for frequencies 20 Hz to 20 kHz rather than equipment designed for infrasound, similar to how one would treat the sound

of hands clapping or birds calling at a repetition rate of a few Hz. To generate audio playback sequences, we used audio field recordings (24-bit, 44.1 kHz, no filtering) of peacock train-rattling displays made using a PMD661 recorder (±1 dB: 20 Hz to 24 kHz; Marantz, New York, NY, USA) and a ME-62 omnidirectional microphone (±2.5 dB: 20 Hz to 20 kHz; Sennheiser, Wedemark, Germany), as described in a previous study (Dakin et al., 2016). Three playback sequences were used (each using sound from a different peacock), with mean rattle repetition rates of 26.7 ± 0.5 Hz; 25.3 ± 0.5 Hz; and 24.6 ± 0.5 Hz. Recordings of train-rattling in the field indicated that rattles are in-phase (i.e., temporally coherent) over bouts approximately 1.2 s duration that are repeated for several minutes during displays (Dakin and Montgomerie, 2009; Dakin et al., 2016). We spliced together bouts with an integer number of rattling periods to form a longer audio playback file with a total duration of approximately 5 min.

All sound files were played back on a Lenovo Thinkpad T460S computer connected to a 402-VLZ4 mixer (Mackie; preamplifier; < 0.0007% distortion 20 Hz to 50 kHz) and a ROKIT 10-3 G3 10" powered studio monitor (KRK Systems, Fort Lauderdale, Florida, USA; ± 2.5 dB over to 40 Hz to 20kHz, –10 dB at 25 Hz relative to ≥ 40 Hz) with a 25.4 cm diameter subwoofer (A = 12.7 cm). Following (Gerhardt, 1992), we examined re-recordings of the playback stimuli made with the same microphone and recorder used for the original field audio recordings, and found that the resulting waveforms and spectrograms (Fig. S2) had the same temporal features (“rattle” notes) as the original field recordings of train-rattling (e.g., Fig. 4A in (Dakin et al., 2016)).

As a control, we played back a Gaussian white noise file generated using MATLAB’s imnoise command (5 min. duration, 24-bit, 44100 Hz, FFT amplitude flat from < 1 Hz to 22,000 Hz computed using a rectangular window to preserve Fourier amplitudes). The white noise playback assessed whether the crest samples could be driven to vibrate measurably by a broadband signal similar to the train-rattles, but lacking the low-frequency amplitude modulation of the train-rattling recording at the “rattle” repetition rate. The root-mean-squared (rms) amplitudes of all playback recordings and the white noise control were scaled to the same value while also ensuring that no clipping occurred at high amplitude. Fig. S2 shows a waveform and spectrogram of a recording of train-rattling and white noise stimuli as they were played back using the audio equipment in the playback experiment.

For playback experiments, the preamplifier volume controls of the mixer were adjusted so that the mean playback SPL was 88 ± 1 dB at 3 m as measured by a Type 2 model R8050 sound level meter (accuracy ±1.4 dB, C-weighting, 30-100 dB, slow 1.0 s setting; Reed Instruments, Wilmington, NC USA). For comparison, previously-reported values for peacock train-rattling mechanical sounds corrected for background noise were given as 67 to 77 dB at R = 3 m (unweighted SPL) (Freeman and Hare, 2015), similar to audible bird wingbeat SPL summarized in Table S2. For our combination of microphone and playback system, the response at 26 Hz was estimated to be reduced by 12.5 dB compared to the audible range; the increase in playback SPL relative to the reported values accommodates for this attenuation. During playbacks, the background noise with no audio was 58 ± 1 dB SPL. We did not expect interference near-field effects to be measurable for our playback system because the train-rattling and white noise recordings were not pure tones, and, as explained earlier, the predicted interference near-field regime is $R < 2\pi A^2/\lambda = 0.7$ cm for 26 Hz. Consistent with this expectation, we found no variation due to interference when we measured SPL at nine different positions across the subwoofer speaker between the center and edges, at distances perpendicular to the speaker between 12.7 cm to 0.5 m.

Female crest samples (n = 3; crests 7, 8, 15) with resonant responses determined in the vibrational dynamics trials were mounted on a tripod at a distance R = A = 12.7 cm away from the subwoofer speaker face to give optimal exposure to the flow near-field (Fig. S2). Vibrational motion of the samples was measured for three separate trials per crest and per recording using high-speed video (reducing speaker volume to zero and waiting > 5 s in between trials), and the crest motions were tracked and analyzed from video using the methods described above. The duration of train-rattling bouts gave an FFT frequency resolution of ± 0.50 Hz for vibrational response analysis. To minimize direct mechanical coupling via the substrate, the crest samples and speaker were mounted on Sorbothane™ vibration-isolation pads. Because peacocks often display near the edges of thick vegetation, next to natural ground slopes, or next to hard walls (Hillgarth, 1984; personal observation), anechoic conditions are not required for effective courtship displays or for simulating their mechanical sounds. However, we still chose to minimize reverberations by surrounding the experiment with acoustic tiles and sound absorbing

sheets (Audimute, Cleveland, OH USA; audible sound reduction rating: SAA 0.68, NRC 0.65), resulting in an SPL decrease of 5 dB when distance was doubled for $R \geq 0.25$ m. This decrease in SPL is intermediate between the free-field value of 6 dB and a typical reflective room value of 3 dB (Toole, 2008). We also performed negative controls to ensure that reverberations and substrate vibrations did not drive crest vibrations. This was accomplished by inserting a foam tile between the crest samples and the speaker to block particle velocity oscillations and attenuate directional sound pressure waves from the speaker. Thus, any crest vibrations measured during the controls would be due to substrate vibrations, reverberations, transmitted sound pressure waves, and/or other environmental sources.

Simulated wing-shaking experiments

High-speed videos from a previous study were used to determine the frequency and amplitude of wing motions during the peacock's wing-shaking display (Dakin et al., 2016). We used four videos filmed with the wingtip motion closely aligned with the image plane (see Movie S1) that also showed tail feathers with known lengths. The amplitude of wing-shaking motion was defined by the mean diameter of motion circumscribed by the tips of the partly-unfurled wings during this display, which we estimated to be 7.6 cm on average (range 5.5 to 10 cm). To simulate the wing motions observed in displaying peacocks and the resulting air motions, we used a robotic mechanism that caused an entire peacock wing to flap with the wing plane held in a fixed vertical orientation while the wingtip circumscribed a circle (Movie S1 and Fig. S3). The peacock wing was mounted on a carbon fiber rod using a balsa wood base that was attached to the wing via adhesive at the shoulder; this rod pivoted about a clevis joint, which allowed the wing axis to move in a vertical circle while the wingspan remained in the vertical plane. At the end opposite the wing, the rod was attached to a circular crank by a universal joint. The crank and attached wing assembly was driven at 4.95 ± 0.05 Hz by a DC motor. While actual wing-shaking involves motion of two wings toward each other, which presumably displaces more air than a single wing, this apparatus used a single flapping wing moving in a slightly larger diameter (14 cm) circle at the wingtips.

To determine how wing-shaking influences the crest of an observing bird, we first determined the location of maximal airflow speed during robotic wing-shaking. Airflow speeds were

measured by a model 405i Wireless Hot-wire Anemometer (Testo, Sparta, NJ, USA) oriented with its sensor facing in the same direction as the crest samples; this device has a resolution of 0.01 m/s, accuracy of 0.1 m/s, measurement rate of 1 Hz, and equilibration time of approximately 5 s. To define the airflow pattern around the flapping wing, air speed was sampled at every point on a 5 cm grid, 5-7 times per location. Based on these results, we determined the angle at which to position the crest sample. Fig. S3 shows how three peahen feather crest samples (Crests 08, 12, and 13) were positioned using a tripod at the vertical midline of the wing located at various distances from the wing-tips. The resulting motion of the crests was then filmed using high-speed video as described above in "Video analysis" to quantify the vibrational response of the three peahen crests. To verify that substrate vibrations did not drive the crest motion, we also performed a control by inserting a 3 x 4 ft foamboard in between the crest and wing to block the airflow from the wing motion; this reduced the root-mean-squared crest motion to 14% of its value with wing motion-induced airflow present. For comparison with the wing-shaking frequency during displays, flapping frequencies during ascending and level flight were also measured for 9 peacocks from 6 online videos (Table S3).

Force measurements

Peacock feather keratin, like other biopolymers, can have a nonlinear elastic response to external stresses (Weiss and Kirchner, 2010). Because the stimuli in the mechanical shaker, audio playback and wing-shaking experiments each exerted different forces and these forces may have had greater magnitudes than those encountered in the field, we wanted to understand how to extrapolate from our laboratory experiments to a lower force regime that is potentially more biologically relevant. Consequently, we measured the elastic mechanical response of peafowl crests to an external bending force applied to the flags of the crest. We studied the static mechanical response of peafowl crests in the single cantilever bending geometry by measuring the relationship between flag displacement and restoring force of the crest in the out-of-plane orientation (Fig. 1D). Force measurements were made using a Model DFS-BTA force sensor (accuracy ± 0.01 N) connected to a LabQuest2 datalogger (Vernier Software & Technology, Beaverton, OR, USA), which was calibrated using known masses. The force sensor was attached to a thin rectangular plastic blade oriented in the horizontal plane. The edge of the blade was pressed against the midpoint of the flags of the vertically oriented crest to measure the

restoring force exerted by the bent crests. The crests were mounted on a micrometer that moved them toward the force sensor and enabled measurement of crest displacement relative to the location at which the crest flag first deformed and the restoring force first became non-zero within measurement error. These measurements were performed for three trials each for three male and three female crest samples. The resulting force vs displacement data were fit to a linear force-displacement model to determine the linearity of elastic bending deformations. This also gave a value of the bending spring constant, k.

Statistical analysis

All measurements and fitted values are reported as means [95% confidence interval, defined as 1.96 × s.e.m. for normally distributed data], unless noted otherwise.

To analyze sources of variation in whole crest f_r and Q, we fit Gaussian linear mixed effects models with a random effect of crest ID to account for repeated measures of each bird's crest using the nlme 3.1-131 package (Pinheiro et al., 2017) in R 3.3.3 (R Core Team, 2017). We first verified that trial order and frequency sweep rate, two aspects of the experimental design, did not have significant effects on either f_r or Q (all $p > 0.28$). The next step was to evaluate the potential effects of morphological traits that could influence crest resonance. Because our sample size was only 15 crests, we considered models with only one morphological trait predictor, selected from the following list: length, width, number of feathers, percent of unaligned feathers, and percent of short feathers. These morphological traits were fitted as fixed effect predictors. All models also included fixed effects of sex as well as the vibration orientation (either in-plane, or out-of-plane). We used AICc to select the best-fit model (Bartoń, 2015) and evaluated significance of the fixed effects using Wald tests. We report $R^2_{\mathrm{LMM(m)}}$ as a measure of the total variance explained by the fixed effects (Nakagawa and Schielzeth, 2013; Bartoń, 2015). We also used the variance components of the best-fit model to calculate the adjusted repeatability, defined as the variance attributed to differences among crests after adjusting for variation explained by the fixed effects (Nakagawa and Schielzeth, 2010). Inspection of the data and model residuals revealed that variance in f_r differed among crests, so when modelling f_r, we specified this heteroscedasticity using the weights argument (Pinheiro et al., 2017).

RESULTS

Morphology

A microscopic examination of peafowl crest feathers reveals that their shafts have associated feathers with the structure of filoplumes at the base (Fig. 1E) that agree in location and morphology with those shown in micrographs of filoplumes cited earlier in the Methods. These were structurally distinct from immature crest feathers, which also retained a sheath until they had grown to a length much greater than that of the filoplumes.

The average lengths of the whole crest samples used in this study were 5.3 [4.8, 5.7] cm for 8 female crests, and 5.4 [5.1, 5.7] cm for 7 male crests. Fig. 2 shows that this range of crest lengths agrees with that of live peafowl, indicating that the crest samples used in these experiments were fully grown (Dakin, 2011). The average widths of the whole crest samples were 5.5 [4.6, 6.3] cm for the female crests, and 6.1 [5.3, 6.9] cm for the male crests. These width values were approximately 20% (female) to 27% (male) smaller than those found on live birds (Fig. 2). This difference could be due to the crest ornament being spread 1-2 cm more in the sagittal plane by muscle action in the live bird, as observed for erectile crest plumage in many other species (Hagelin, 2002), in addition to the effect of skin drying.

All 7 of the male crest samples had feathers of uniform length, defined as ±8% of the mean fully-grown crest feather length. This is also typically observed *in vivo*, where 72% of male *P. cristatus* crests studied in (Dakin, 2011) had feathers of uniform length. In contrast, the majority (6/8, or 75%) of the female crest samples had non-uniform feather lengths (using the same definition above), which was again similar to the previous *in vivo* study, where 77% of females had non-uniform crest feather lengths (Dakin, 2011). On average, the dried female crests had 7.0% [2.1, 11.8] of their feathers shorter than the mean fully-grown crest feather length. Eight out of the 15 crest samples had all feathers oriented in the same plane within ±5º; five of the crests had 7-11% of the feathers unaligned, and two male crests had 22% and 50% unaligned feathers, respectively.

We also studied the morphology of individual peafowl crest feathers to understand their unusual structure (Fig. 1C). The average rachis tapered evenly over its 39.90 [38.89, 40.91] mm length and had a mass of 5.1 [4.8, 5.3] mg, and the plume (or flag) added another 2.50 [0.87, 4.06] mg. Unlike the fully formed barbs in the pennaceous flag, the lower barbs were short (4.1 [3.0, 5.2] mm) and lacked barbules altogether.

Vibrational Dynamics

The vibrational drive transfer functions of peafowl crests had either a single dominant fundamental peak, or in a few cases, a cluster of two to three peaks in a narrowly-defined frequency range, with no evidence that other modes of vibration caused detectable motions of the pennaceous flags. Each main peak agreed well with the expected Lorentzian fit function (mean adjusted-R^2 = 0.97; range [0.91, 0.998]), supporting our choice of shaker amplitudes and frequency sweep rates (Fig. 3A). The value of $f_r \pm \Delta f/2$ defines the approximate range of drive frequencies over which power is efficiently coupled into the oscillator. Fig. 3B shows that shaking frequencies measured in the field for displaying male and female peafowl (Dakin et al., 2016) lay within $f_r \pm \Delta f/2$ of the crest resonant frequency for both sexes (n = 8 female crests and 7 male crests). When the shaking force was oriented out-of-plane, the mean crest resonant frequency, f_r, was 28.1 [28.0, 28.1] Hz for female and 26.3 [25.9, 26.6] Hz for male crests, respectively. The mean Δf values were 6.2 [4.4,8.0] Hz (females) and 4.3 [4.2, 4.4] Hz (males).

The repeatability of f_r for whole crests was very high at 94%, demonstrating strong and consistent differences among individual crests (Fig. 3B). Analysis of the sources of variation in f_r indicated that 28% of the total variation in f_r could be explained by sex, crest orientation, and the total area of the pennaceous flags (Fig. 3B). The effect of crest orientation was strong and significant, such that out-of-plane vibrations have f_r values approximately 2.4 Hz higher on average ($p < 0.0001$), whereas the sex difference was not significant ($p = 0.87$) and crests with reduced flag area have a slight but non-significant tendency to have higher f_r values ($p = 0.10$). Crest length, width, number of feathers, and the percent of unaligned and short feathers did not explain variation among crests in the value of f_r. The frequency response of individual crest feathers was generally consistent with that of the whole/intact crests, as the resonant frequencies of these feathers in the out-of-plane orientation ranged from 19.2 Hz to 32.4 Hz (Fig. 3B).

Fig. 3C shows a comparison of the fundamental frequency of out-of-plane vibrations vs rachis length for peafowl crests and individual crest feathers, three other types of short peacock feathers, and crest feathers for four other species of birds.

The sharpness of the crest's resonant frequency is indicated by the quality factor, Q (Fig. 3D). The mean Q for peafowl crests vibrated in the out-of-plane orientation (4.8 [4.0, 5.6] for females, 6.2 [5.6, 6.9] for males) was intermediate between that of peafowl eyespot feathers (Q = 3.6-4.5 ± 0.4 and 1.8 ± 0.3, for individual feathers and feather arrays, respectively) and the tail feathers that drive the shaking, for which Q_1 = 7.8 ± 0.5 (Dakin et al., 2016). This indicates that peafowl crests are moderately sharply-tuned resonators. We discuss the effect of the level of damping due to these values of Q on the time behavior of feather vibrations below. The natural frequency of an undriven oscillator is related to its resonant frequency by $f_o = f_r \text{ sqrt}(1 - ½ Q^{-2})$; for our measured values of Q for peafowl crests, this means that the resonant frequency is shifted from the natural frequency by an undetectably small amount (≤ 1.2%) relative to measurement error. Thus, peafowl feather crests should vibrate at approximately the same frequency during either undriven or driven oscillations. We will return to this point in the discussion of the wing-shaking display simulation experiment.

The repeatability of Q was estimated at 47%, indicating moderate differences among crests in Q. Approximately 49% of the variation in crest Q could be explained by sex, crest orientation, and the total area of the pennaceous flags (Fig. 3D). Male crests were significantly more sharply-tuned than those of females ($p < 0.0001$), and crests that had less flag area tended to be more sharply-tuned ($p = 0.03$). Peafowl crests also have more sharply-tuned resonance when they are vibrated out-of-plane ($p < 0.0001$) as compared to the in-plane orientation.

Note that the complete analysis of vibration data can be reproduced using data and code available at: https://doi.org/10.6084/m9.figshare.5451379.v5 (Dakin et al., 2018).

Force impulse experiments

When ring-shaped air vortices impacted the crests, the barbs responded with clearly visible motion on video with the average amplitude of motion at the flags of 9.4 [4.3, 14.4] mm (Fig. 4A). Analysis of the free vibrational displacement of the crests over time revealed an exponentially decaying sinusoidal response with a mean frequency that agreed within $\leq \pm 0.4\ \Delta f$ of the natural frequency predicted from the measured resonant response of each crest (Fig. 4B), providing a confirmation of our methodology for measuring resonant frequency. Thus, vortices cause the feather crest to vibrate at its natural frequency, with a decrease in amplitude of 13% after 0.2 s, the approximate period of peafowl wing-shaking displays.

Audio playback experiments

An example FFT power spectrum for the vibrational response of a peahen crest sample during audio playback is shown in Fig. 5. For train-rattling audio playback experiments in which the peahen crest samples were located in the flow near-field of the speaker, the vibrational power spectra of the samples had a peak well above noise near the playback train-rattling repetition rate (the effective drive frequency). However, when the white noise recording was played back, the spectral power near the drive frequency was < 4.3% of that found during playbacks. The peak frequency of crest vibrations agreed with the playback train-rattling repetition rate to within 95% CI for all measurements but one, for which it lay within 2.5 s.e.m. Measurements of crest vibrations made with an acoustic foam tile between the speaker and sample had < 11 % of the FFT spectral power at the drive frequency compared to measurements made without the foam; this value placed an upper bound on the contribution of background sources (e.g., room reverberations, substrate vibrations, etc.) that were not associated with particle-velocity oscillations from the playback stimulus.

Wing-shaking experiments and wing-flapping during flight

The simulated wing-shaking experiment resulted in an airflow pattern with speeds ≤ 0.3 m/s. We used the measured positions of maximum airflow speed to determine the locations for three female crest samples for vibrational motion studies. The FFT power spectra of the crest flag vibrational motion had a single peak above the background noise at a frequency that agreed with

the wing-shaking frequency within 95% CI (Fig. 6) for distances up to 90 cm (one sample) and 80 cm (two samples) from the mean wingtip position.

The average peacock wing-flapping frequency during ascending and level flight was 5.5 [5.0, 6.1] Hz (Table S3). This frequency agrees with the average frequency of 5.4 Hz (range of individual bird means = 4.5-6.8 Hz) found for wing-shaking display frequencies measured in the field (Dakin et al., 2016).

Mechanical bending properties

All feather crests exhibited a highly linear elastic response in the bending experiments: force and displacement were linearly related for displacements up to 10.1 [9.1, 11.0] mm (adjusted R^2 = 0.983 [0.978, 0.989]. This allowed us to compute the bending spring constant, k, from the fitted slopes (Fig. S4). The mean bending spring constants for the individual crests ranged from 0.0022 to 0.0054 N/mm with a measurement repeatability of 47% due to the force sensor contacting the crest flag at somewhat different positions during different trials.

DISCUSSION

As found in live birds (Dakin, 2011), the peafowl crest samples were found to be relatively uniform in length and area, which helps explain their relatively well-defined and narrow vibrational resonances (Fig. 3A). The fundamental resonant vibrational frequencies of peafowl crests were also found to agree closely with the frequencies used during male train-rattling and female tail-rattling displays. Are these vibrational responses typical of other peafowl feathers and/or other avian crest feathers? Fig. 3C shows that the resonant frequencies of peafowl crests do not agree within measurement uncertainty with those of three other types of peafowl feathers, nor do they agree with those of crest feathers from four other bird species. This makes it unlikely that the close frequency match between peafowl displays and crest resonance occurs by chance, as that resonant frequency is not what one would expect for a generic peafowl feather or a generic crest feather. We therefore hypothesize that this frequency match has functional significance during multimodal courtship displays.

Our results also demonstrate similarity of both the resonant frequency and the *Q* factor of the peafowl crest's vibrational response with those of the train feathers producing the shaking display. This implies that the peafowl's crest would be well-matched to the train's mechanical sound, but not to environmental sources of noise (Fletcher, 1992). In agreement with this result, we found that exposing peahen crest samples to the near-field of audio playbacks of train-rattling sounds caused the crests to vibrate detectably on video at their resonant frequency (Fig. 5). By contrast, exposing crest samples to white noise resulted in no measurable vibrations above background noise levels. Our measurements of vibrational responses during audio playback were limited to relatively large amplitudes and small distances compared to the very small thresholds found for other mechanoreceptors *in vivo*, and consequently to relatively small source-receiver distances. However, the low thresholds found for mechanosensation *in vivo* suggest that the actual detection range could be much greater than our *in vitro* limits. For example, pigeons can detect submicron threshold vibrational amplitudes applied to flight feathers (Shen, 1983; Hörster, 1990), mammalian hair cells are sensitive to sub-nanometer displacements and 0.01 deg rotations (Crawford and Fettiplace, 1985), tactile receptors in human skin are sensitive to submicron vibrational amplitudes (Löfvenberg and Johansson, 1984), and insect filiform hairs are sensitive to airspeeds as low as 0.03 mm s^{-1} (Shimozawa et al., 2003). This idea also is supported by our measured linear elastic response of feather crests to bending (Fig. S4), which indicates that our results can be extrapolated linearly to lower magnitude stimuli corresponding to larger source-sample separation than those measured here during the audio playback experiments. Further histological and electrophysiological studies of the receptors at the base of avian crest feathers and their associated filoplumes are needed to determine whether these crests can in fact function as sensors that are sensitive to airborne stimuli like the ones studied here.

To understand the vibrational response of peafowl crests to impulsive airflows, we also measured the deflection of peafowl crests when they were struck by individual air ring vortices (Fig. 4). We found that each impulsive stimulus generated a distinct crest response in which the crest feathers vibrated at their natural fundamental frequency briefly before decaying to zero. These results also provided two confirmations of our resonant response data: 1) the agreement between the frequency of these free oscillations and the measured resonant frequency, and 2) the

agreement of the damping time for free vibrations with that expected from the measured *Q* values. Airflows due to wing-shaking motions in the laboratory drove measurable transient crest deflections at distances ≤ 90 cm from the crest (Fig. 6), similar to the lower end of male-female separations in the field during such displays. As explained above, the measured elastic response data suggest this result can be extrapolated to greater distances as well. These findings imply that the airflow impulses generated by *in vivo* wing-shaking displays could stimulate the feather crests of nearby female by producing a series of distinct vibrational responses at the display frequency.

Given that feathers are known to function as airflow sensors during flight, it is easy to imagine how they also could be adapted to function as sensors during social signaling. For example, during social displays, many birds flap or vibrate their wings or tails (Bostwick et al., 2009; Clark et al., 2013; Ota et al., 2015; Clark, 2016; Dakin et al., 2016), producing dynamic visual stimuli as well as mechanical sound and periodic air flow stimuli. Thus, these multimodal displays have the potential to stimulate multiple senses, including vision, hearing (sound pressure waves reception) and vibrotactile perception (i.e., sensing sound air particle velocity or airflow impulses via feather vibrations or deflections). These stimuli may also provide honest signals of male quality. For example, we can hypothesize that air-borne stimuli generated by train- or tail vibrating or shaking displays provide females with an indication of male muscle power and endurance, or that stimuli generated by wing-shaking displays serve as signals of flight muscle performance (Clark, 2016). An alternative hypothesis is that male displays have been selected to match and stimulate pre-existing mechanosensory properties of the female crest, without any benefits to females of this close match. Yet another non-exclusive hypothesis is that both males and females experience crest vibrations driven by body oscillations due to their own train- and tail-rattling displays as a form of proprioception.

Although we have demonstrated here that peafowl crest feathers are effectively stimulated by airborne stimuli during social displays, we do not yet know whether this has behavioral or social significance. Testing this hypothesis requires *in vivo* behavioral experiments. In peafowl, a first step would be to blindfold females and test whether airborne stimuli at the socially salient frequencies elicit a behavioral response. Further experiments could test the function of the crest

during male courtship displays by removing or altering the female crest and then examining how females respond to male displays. One way to do this would be to apply a thin coat of clear varnish to the rachis of the crest feathers; this would stiffen the rachis and increase resonant frequency without affecting the crest's visual appearance (i.e., size or flag iridescence). Similar manipulations could also test whether peacocks use proprioception from the crest to modulate their own vibration displays. The movement of females during displays could also be examined in relation to the airflow patterns generated by wing-shaking peacocks, to test whether female movements are correlated with specific airflows generated by the males. These correlative results could then be tested experimentally by measuring the behavioral response of peahens to oscillatory air flows modulated at frequencies close to and distinct from their crest resonance, to see how this influences attention and body orientation. Because audible sound cues are omnidirectional, these responses could be distinguished from hearing-induced behaviors by comparing results when air flows are directed toward and away from specific regions of the birds' plumage.

The biomechanical properties of the peafowl's crest also suggest a novel design for making sensitive biomimetic detectors for sensing impulsive or periodic airflows. Such devices are required for proposed robotic applications of air vortex rings and other airflow signals as a communication channel (Russell, 2011). The addition of an extremely lightweight pennaceous flag to a cantilever made from a resistance-based flex sensor would enable the flex sensor to experience a large torque from a small force, with a minimal increase in mass.

Thus far, the elaborate shape, size and color of many bird feather crests has led to an emphasis on their visual appearance (reviewed in Seneviratne and Jones, 2008). However, many avian courtship displays also involve wing-shaking, tail-fanning and mechanical sound production that may be detected by nearby females in the vibrotactile channel. For example, we have compiled a list of at least 35 species distributed over 10 avian orders that have crests and perform these types of displays (Table S4). Given the growing interest in multisensory signaling, it seems worth pursuing behavioral studies to investigate whether mechanosensory stimulation enhances the reception of visual and acoustic cues during this multimodal display. The close match between the resonant frequencies found here for peafowl crests and this species' social displays suggest

that it is time to explore a new hypothesis that birds receive and respond to vibrotactile cues in a wider variety of scenarios.

FIGURE LEGENDS

Fig. 1. Morphology of peafowl crests and crest feathers. (A) A peahen (foreground) with the plane of her crest oriented towards the displaying peacock (background) as he performs train-rattling vibrations. (B) Both sexes have a crest with an inverted pendulum shape made up of between 20-31 feathers. This photo shows an adult male measured *in vivo*. (C) A single crest feather showing the pennaceous flag at the distal end. Note that only short, thin barbs are present on the relatively bare rachis (shaft) at the proximal end. (D) A whole crest sample mounted for the laboratory experiments. The two axes of vibrational motions ("in-plane" and "out-of-plane") are indicated. (E) Mechanosensory filoplumes (circled) are located at the base of the peafowl crest feathers.

Fig. 2. Length and width of the whole crest samples as compared to live peafowl crests. Crests (n = 8 female, n = 7 male) measured *in vivo* (means shown to the right of each data column) had similar morphology to the dried samples, except that the crests on live birds tended to be wider. Dried sample dimensions were measured to the nearest 0.1 cm. Each crest sample is indicated by a unique symbol-color combination.

Fig. 3. Vibrational resonance properties of peafowl crests and individual crest feathers. (A) Vibrational spectrum and Lorentzian fit for peacock crest sample Crest 01. (B-D) Data on the mean crest resonant frequencies, f_r, and quality factors, Q. Each dried crest sample (n = 8 female, n = 7 male) is indicated by a unique symbol-color combination, consistent with Fig. 2. (B) The mean resonant frequencies, f_r, of the crest are a close match for the range of vibrational frequencies used during peafowl social displays. As an indication of measurement error, the average 95% CI for each mean f_r estimate spans 0.072 Hz. The gray shaded area is the range of vibrational frequencies of the train-rattling display, with dotted lines showing the means for displays performed by peacocks (blue) and peahens (green) (Dakin et al., 2016). Variation in f_r was influenced by the vibrational orientation and was also associated with the sex of the bird and the area of pennaceous flags at the top of the crest (although the association with flag area was not statistically significant). The first panel in (B) also shows how a small sample of single crest feathers (n = 3 from male Crest 03, n = 5 from male Crest 05, and n = 3 from female Crest 10)

had a similar range of resonant frequencies as the whole crests vibrated in the same out-of-plane orientation. (C) Fundamental frequency for vibrations in the out-of-plane orientation for peafowl crest and non-crest feathers with similar lengths and crest feathers from four non-peafowl species described in Table S1 and Fig. S1. Means for male and female peafowl crests are both plotted. The y-axis of (C) is aligned with that of (B) for comparison. (D) The mean quality factor, *Q*, was also influenced by the vibrational orientation, and was associated with the sex of the bird and the area of pennaceous flags. The average 95% CI for each mean *Q* estimate spanned 0.233. Black horizontal lines in (B) and (D) are grand means.

Fig. 4. Displacement of the crest in response to air vortices. (A) Time series showing the change in flag position after a peacock crest (Crest 09) was impacted by a moving vortex of air. When peafowl crests were impacted by such air ring vortices, they deflected measurably, oscillating at their resonant frequency with an amplitude that decayed to a few percent of the initial value over the period of the peacock's wing-shaking display. (B) Mean resonant frequencies (f_r) and mean vortex response frequencies (± 95% CI) for three crests in the vortex experiment.

Fig. 5. Effect of audio playback on crests. Vibrational response of a peahen crest (Crest 08) exposed to audio playback in the near-field of the speaker. The FFT spectral power during playback of train-rattling sound (dotted line, plotted on a linear scale on the y-axis) has a peak near the resonant frequency of the crest. The spectral power values recorded during white noise playback (solid line) and when the train-rattling audio was blocked by a foam tile (red dashed line) are also shown.

Fig. 6. Effects of simulated wing-shaking displays. Vibrational response of a female peahen crest (Crest 13) exposed to airflow from a robot that simulated 5.0 Hz peacock wing-shaking displays at a distance 50 cm from the moving wingtip (see also Fig. S3). Note that the FFT spectral power (y-axis) is plotted on a linear scale.

Acknowledgments

We are grateful to Maarten Hesseling for assistance with preliminary vibrational measurements, Robert Beyer, Robert Lukasik, and Roger Hill for help with instrumentation design and construction, Kate Davidson (Siskiyou Aviary) for feather samples, and Robert Koch, Holger Klinck, and Carr Everbach for advice about reproducing low repetition rate sounds. We thank two anonymous reviewers and James Hare for helpful comments on an earlier version of the manuscript.

Competing interests

The authors declare no competing or financial interests.

Author contributions

Conceptualization: S.A.K.; Methodology: S.A.K., D.V.; Investigation: S.A.K., D.V.; Data curation: S.A.K., D.V., R.D.; Analysis: S.A.K., R.D., D.V.; Writing – original draft: S.A.K., R.D.; Writing – review & editing: S.A.K., R.D., D.V.

Funding

This work was supported by Haverford College and a National Sciences and Engineering Research Council of Canada (NSERC) Postdoctoral Fellowship to R.D.

Data availability

All data and code necessary to reproduce the results of this study are available at: https://doi.org/10.6084/m9.figshare.5451379.v5

References

Barth, F. G. (2013). *A spider's world: senses and behavior*. Springer Science & Business Media.

Barth, F. G. (2014). The Slightest Whiff of Air: Airflow Sensing in Arthropods. In *Flow Sensing in Air and Water*, pp. 169–196. Berlin: Springer.

Barth, F. G., Humphrey, J. A. C. and Srinivasan, M. V. (2012). *Frontiers in Sensing: From Biology to Engineering*. Berlin: Springer Science & Business Media.

Bartoń, K. (2015). *MuMIn 1.15.6*.

Biewener, A. A. and Full, R. J. (1992). Force platforms and kinematic analysis. In *Biomechanics - Structures and Systems: A Practical Approach* (ed. Biewener, A. A.), p. IRL Press.

Bilo, D. and Bilo, A. (1978). Wind stimuli control vestibular and optokinetic reflexes in the pigeon. *Naturwissenschaften* **65**, 161–162.

Bilo, D. and Bilo, A. (1983). Neck flexion related activity of flight control muscles in the flow-stimulated pigeon. *J. Comp. Physiol.* **153**, 111–122.

Blackstock, D. T. (2000). *Fundamentals of Physical Acoustics*. New Jersey, USA: John Wiley & Sons.

Bleckmann, H., Mogdans, J. and Coombs, S. L. (2014). *Flow sensing in air and water*. Berlin, Germany: Springer.

Bostwick, K. S., Elias, D. O., Mason, A. and Montealegre-Z, F. (2009). Resonating feathers produce courtship song. *Proc. R. Soc. Lond. B Biol. Sci.* rspb20091576.

Bradbury, J. W. and Vehrencamp, S. L. (2011). In *Principles of Animal Communication*, p. page 30. Sunderland, USA: Sinauer.

Brown, R. E. and Fedde, M. R. (1993). Airflow sensors in the avian wing. *J. Exp. Biol.* **179**, 13–30.

Brücker, C., Schlegel, D. and Triep, M. (2016). Feather vibration as a stimulus for sensing incipient separation in falcon diving flight. *Nat. Resour.* **07**, 411.

Burley, N. T. and Symanski, R. (1998). "A taste for the beautiful": Latent aesthetic mate preferences for white crests in two species of Australian grassfinches. *Am. Nat.* **152**, 792–802.

Childress, R. B. and Bennun, L. A. (2002). Sexual character intensity and its relationship to breeding timing, fecundity and mate choice in the great cormorant *Phalacrocorax carbo lucidus*. *J. Avian Biol.* **33**, 23–30.

Clark, C. J. (2016). Locomotion-induced Sounds and Sonations: Mechanisms, Communication Function, and Relationship with Behavior. In *Vertebrate Sound Production and Acoustic Communication*, pp. 83–117. Switzerland: Springer, Cham.

Clark, G. A. and de Cruz, J. B. (1989). Functional interpretation of protruding filoplumes in oscines. *The Condor* **91**, 962–965.

Clark, C. J., Elias, D. O., Girard, M. B. and Prum, R. O. (2013). Structural resonance and mode of flutter of hummingbird tail feathers. *J. Exp. Biol.* **216**, 3404–3413.

Clark, C. J., Mountcastle, A. M., Mistick, E. and Elias, D. O. (2017). Resonance frequencies of honeybee (*Apis mellifera*) wings. *J. Exp. Biol.* **220**, 2697–2700.

Cornec, C., Hingrat, Y., Aubin, T. and Rybak, F. (2017). Booming far: the long-range vocal strategy of a lekking bird. *Open Sci.* **4**, 170594.

Crawford, A. C. and Fettiplace, R. (1985). The mechanical properties of ciliary bundles of turtle cochlear hair cells. *J. Physiol.* **364**, 359–379.

Cummins, B. and Gedeon, T. (2012). Assessing the Mechanical Response of Groups of Arthropod Filiform Flow Sensors. In *Frontiers in Sensing*, pp. 239–250. Springer, Vienna.

Cunningham, S. J., Alley, M. R. and Castro, I. (2011). Facial bristle feather histology and morphology in New Zealand birds: Implications for function. *J. Morphol.* **272**, 118–128.

Dakin, R. (2011). The crest of the peafowl: a sexually dimorphic plumage ornament signals condition in both males and females. *J. Avian Biol.* **42**, 405–414.

Dakin, R. and Montgomerie, R. (2009). Peacocks orient their courtship displays towards the sun. *Behav. Ecol. Sociobiol.* **63**, 825–834.

Dakin, R. and Montgomerie, R. (2011). Peahens prefer peacocks displaying more eyespots, but rarely. *Anim. Behav.* **82**, 21–28.

Dakin, R., McCrossan, O., Hare, J. F., Montgomerie, R. and Kane, S. A. (2016). Biomechanics of the peacock's display: How feather structure and resonance influence multimodal signaling. *PLOS ONE* **11**, e0152759.

Dakin, R., van Beveren, D. and Amador Kane, S. (2018). Statistical supplement to: Biomechanics of the peafowl's crest reveals frequencies tuned to social displays. https://doi.org/10.6084/m9.figshare.5451379.v5.

Dambach, M., Rausche, H.-G. and Wendler, G. (1983). Proprioceptive feedback influences the calling song of the field cricket. *Naturwissenschaften* **70**, 417–418.

De Bree, H.-E., Svetovoy, V., Raangs, R. and Visser, R. (2004). The very near field: theory, simulations and measurements of sound pressure and particle velocity in the very near field.p. St. Petersburg, Russia.

Dent, M. L., Klump, G. M. and Schwenzfeier, C. (2002). Temporal modulation transfer functions in the barn owl (*Tyto alba*). *J. Comp. Physiol. A* **187**, 937–943.

Dirks, J.-H. and Dürr, V. (2011). Biomechanics of the stick insect antenna: Damping properties and structural correlates of the cuticle. *J. Mech. Behav. Biomed. Mater.* **4**, 2031–2042.

Dooling, R. J. and Searcy, M. H. (1981). Amplitude modulation thresholds for the parakeet (*Melopsittacus undulatus*). *J. Comp. Physiol*. **143**, 383–388.

Fahy, F. J. (2001). *Foundations of Engineering Acoustics*. London: Academic Press.

Ferrer, B., Espinosa, J., Roig, A. B., Perez, J. and Mas, D. (2013). Vibration frequency measurement using a local multithreshold technique. *Opt. Express* **21**, 26198–26208.

Fletcher, N. H. (1992). *Acoustic Systems in Biology*. New York, USA: Oxford University Press.

Freeman, A. R. and Hare, J. F. (2015). Infrasound in mating displays: a peacock's tale. *Anim. Behav.* **102**, 241–250.

Gao, J., Chu, J., Shang, H. and Guan, L. (2015). Vibration attenuation performance of long-eared owl plumage. *Bioinspired Biomim. Nanobiomaterials* **4**, 187–198.

Gerhardt, H. C. (1992). Conducting Playback Experiments and Interpreting their Results. In *Playback and Studies of Animal Communication*, pp. 59–77. Boston, MA: Springer.

Greenfield, M. D. (2002). *Signalers and Receivers: Mechanisms and Evolution of Arthropod Communication*. New York, USA: Oxford University Press.

Hagelin, J. C. (2002). The kinds of traits involved in male-male competition: a comparison of plumage, behavior, and body size in quail. *Behav. Ecol.* **13**, 32–41.

Hans, H., Miao, J. M. and Triantafyllou, M. S. (2014). Mechanical characteristics of harbor seal (*Phoca vitulina*) vibrissae under different circumstances and their implications on its sensing methodology. *Bioinspir. Biomim.* **9**, 036013.

Hart, N. S. (2002). Vision in the peafowl (Aves: *Pavo cristatus*). *J. Exp. Biol.* **205**, 3925–3935.

Hartmann, M. J., Johnson, N. J., Towal, R. B. and Assad, C. (2003). Mechanical characteristics of rat vibrissae: resonant frequencies and damping in isolated whiskers and in the awake behaving animal. *J. Neurosci.* **23**, 6510–6519.

Heidelbach, J. and Dambach, M. (1997). Wing-flick signals in the courtship of the African cave cricket, *Phaeophilacris spectrum*. *Ethology* **103**, 827–843.

Heinzel, H.-G. and Dambach, M. (1987). Travelling air vortex rings as potential communication signals in a cricket. *J. Comp. Physiol. A* **160**, 79–88.

Hillgarth, N. (1984). Social organization of wild peafowl in India. *World Pheas. Assoc. J.* **9**, 47–56.

Hörster, W. (1990). Vibrational sensitivity of the wing of the pigeon (*Columba livia*) — a study using heart rate conditioning. *J. Comp. Physiol. A* **167**, 545–549.

Imber, M. J. (1971). Filoplumes of petrels and shearwaters. *N. Z. J. Mar. Freshw. Res.* **5**, 396–403.

James, P. C. (1986). The filoplumes of the Manx Shearwater *Puffinus puffinus*. *Bird Study* **33**, 117–120.

Jones, I. L. and Montgomerie, R. (1992). Least auklet ornaments: do they function as quality indicators? *Behav. Ecol. Sociobiol.* **30**, 43–52.

Kalmijn, A. J. (1988). Hydrodynamic and Acoustic Field Detection. In *Sensory Biology of Aquatic Animals*, pp. 83–130. New York, USA: Springer.

Kämper, G. and Dambach, M. (1981). Response of the cercus-to-giant interneuron system in crickets to species-specific song. *J. Comp. Physiol.* **141**, 311–317.

Kirchner, W. H. (1994). Hearing in honeybees: the mechanical response of the bee's antenna to near field sound. *J. Comp. Physiol. A* **175**, 261–265.

Klump, G. M. and Okanoya, K. (1991). Temporal modulation transfer functions in the European Starling (*Sturnus vulgaris*): I. Psychophysical modulation detection thresholds. *Hear. Res.* **52**, 1–11.

Larsen, O. N. and Wahlberg, N. (2017). Sound and Sound Sources. In *Comparative Bioacoustics: An Overview* (ed. Brown, C.) and Riede, T.), pp. 3–61. Sharjah, UAE: Bentham Science Publishers.

Li, Q., Gao, K.-Q., Vinther, J., Shawkey, M. D., Clarke, J. A., D'Alba, L., Meng, Q., Briggs, D. E. G. and Prum, R. O. (2010). Plumage color patterns of an extinct dinosaur. *Science* **327**, 1369–1372.

Lindow, B. E. K. and Dyke, G. J. (2006). Bird evolution in the Eocene: climate change in Europe and a Danish fossil fauna. *Biol. Rev.* **81**, 483–499.

Löfvenberg, J. and Johansson, R. S. (1984). Regional differences and interindividual variability in sensitivity to vibration in the glabrous skin of the human hand. *Brain Res.* **301**, 65–72.

Lucas, A. M. and Stettenheim, P. R. (1972). Structure of Feathers. In *Avian Anatomy: Integument*, pp. 341–419. Washington, DC: US Department of Agriculture.

Lunichkin, A. M., Zhemchuzhnikov, M. K. and Knyazev, A. N. (2016). Basic elements of behavior of the cricket *Phaeophilacris bredoides Kaltenbach* (Orthoptera, Gryllidae). *Entomol. Rev.* **96**, 537–544.

Magal, C., Dangles, O., Caparroy, P. and Casas, J. (2006). Hair canopy of cricket sensory system tuned to predator signals. *J. Theor. Biol.* **241**, 459–466.

Markl, H. (1983). Vibrational Communication. In *Neuroethology and Behavioral Physiology*, pp. 332–353. Berlin: Springer.

Nakagawa, S. and Schielzeth, H. (2010). Repeatability for Gaussian and non-Gaussian data: a practical guide for biologists. *Biol. Rev.* **85**, 935–956.

Nakagawa, S. and Schielzeth, H. (2013). A general and simple method for obtaining R2 from generalized linear mixed-effects models. *Methods Ecol. Evol.* **4**, 133–142.

Necker, R. (1985a). Receptors in the skin of the wing of pigeons and their possible role in bird flight. In *Biona Report* (ed. Nachtigall, W.), pp. 433–444. Stuttgart, New York: Fischer.

Necker, R. (1985b). Observations on the function of a slowly-adapting mechanoreceptor associated with filoplumes in the feathered skin of pigeons. *J. Comp. Physiol. A* **156**, 391–394.

Neimark, M. A., Andermann, M. L., Hopfield, J. J. and Moore, C. I. (2003). Vibrissa resonance as a transduction mechanism for tactile encoding. *J. Neurosci.* **23**, 6499–6509.

O'Neil, N. P., Charrier, I. and Iwaniuk, A. N. (2018). Behavioural responses of male ruffed grouse (*Bonasa umbellus, L.*) to playbacks of drumming displays. *Ethology* **124**, 161–169.

Ota, N., Gahr, M. and Soma, M. (2015). Tap dancing birds: the multimodal mutual courtship display of males and females in a socially monogamous songbird. *Sci. Rep.* **5**,.

Paton, J. A., Capranica, R. R., Dragsten, P. R. and Webb, W. W. (1977). Physical basis for auditory frequency analysis in field crickets (Gryllidae). *J. Comp. Physiol.* **119**, 221–240.

Paunescu, G., Lutzmann, P., Göhler, B. and Wegner, D. (2015). Comparison of high speed imaging technique to laser vibrometry for detection of vibration information from objects. In *Electro-Optical Remote Sensing, Photonic Technologies, and Applications IX*, p. 96490D. International Society for Optics and Photonics.

Persons, W. S. and Currie, P. J. (2015). Bristles before down: A new perspective on the functional origin of feathers. *Evolution* **69**, 857–862.

Pinheiro, J., Bates, D., DebRoy, S. and Sarkar, D. (2017). *nlme 3.1-131: linear and nonlinear mixed effects models*.

R Core Team (2017). *R 3.3.3: A Language and Environment for Statistical Computing*. Vienna, Austria: R Foundation for Statistical Computing.

Rogers, P. H. and Cox, M. (1988). Underwater Sound as a Biological Stimulus. In *Sensory Biology of Aquatic Animals*, pp. 131–149. Springer, New York, NY.

Russell, R. A. (2011). Air vortex ring communication between mobile robots. *Robot. Auton. Syst.* **59**, 65–73.

Santer, R. D. and Hebets, E. A. (2008). Agonistic signals received by an arthropod filiform hair allude to the prevalence of near-field sound communication. *Proc. R. Soc. Lond. B Biol. Sci.* **275**, 363–368.

Saxod, R. (1978). Development of Cutaneous Sensory Receptors Birds. In *Development of Sensory Systems*, pp. 337–417. Berlin: Springer.

Seneviratne, S. S. and Jones, I. L. (2008). Mechanosensory function for facial ornamentation in the whiskered auklet, a crevice-dwelling seabird. *Behav. Ecol.* **19**, 784–790.

Seneviratne, S. S. and Jones, I. L. (2010). Origin and maintenance of mechanosensory feather ornaments. *Anim. Behav.* **79**, 637–644.

Shatz, L. F. and Groot, T. D. (2013). The frequency response of the vibrissae of harp seal, <i>Pagophilus groenlandicus<i>, to sound in air and water. *PLOS ONE* **8**, e54876.

Shen, J.-X. (1983). A behavioral study of vibrational sensitivity in the pigeon (*Columba livia*). *J. Comp. Physiol.* **152**, 251–255.

Shimozawa, T., Murakami, J. and Kumagai, T. (2003). Cricket Wind Receptors: Thermal Noise for the Highest Sensitivity Known. In *Sensors and Sensing in Biology and Engineering*, pp. 145–157. Berlin: Springer.

Sisneros, J. A. (2015). *Fish Hearing and Bioacoustics: An Anthology in Honor of Arthur N. Popper and Richard R. Fay.* Berlin: Springer.

Smith, W. F. (2010). *Waves and Oscillations: A Prelude to Quantum Mechanics*. New York, USA: Oxford University Press.

Sofroniew, N. J. and Svoboda, K. (2015). Whisking. *Curr. Biol.* **25**, R137–R140.

Stettenheim, P. R. (2000). The integumentary morphology of modern birds—an overview. *Am. Zool.* **40**, 461–477.

Sueur, J., Windmill, J. F. C. and Robert, D. (2010). Sound emission and reception tuning in three cicada species sharing the same habitat. *J. Acoust. Soc. Am.* **127**, 1681–1688.

Sullivan, T. N., Wang, B., Espinosa, H. D. and Meyers, M. A. (2017). Extreme lightweight structures: avian feathers and bones. *Mater. Today* **20**, 377–391.

Tautz, J. and Markl, H. (1978). Caterpillars detect flying wasps by hairs sensitive to airborne vibration. *Behav. Ecol. Sociobiol.* **4**, 101–110.

Taylor, A. M., Bonser, R. H. C. and Farrent, J. W. (2004). The influence of hydration on the tensile and compressive properties of avian keratinous tissues. *J. Mater. Sci.* **39**, 939–942.

Toole, F. E. (2008). *Sound Reproduction: Loudspeakers and Rooms*. Oxford, UK: Focal Press.

Tsujiuchi, S., Sivan-Loukianova, E., Eberl, D. F., Kitagawa, Y. and Kadowaki, T. (2007). Dynamic range compression in the honey bee auditory system toward waggle dance sounds. *PLOS ONE* **2**, e234.

Weir, K. A. and Lunam, C. A. (2011). The Structure and Sensory Innervation of the Integument of Ratites. In *The Welfare of Farmed Ratites*, pp. 131–145. Berlin: Springer.

Weiss, I. M. and Kirchner, H. O. K. (2010). The peacock's train (*Pavo cristatus* and *Pavo cristatus mut. alba*) I. structure, mechanics, and chemistry of the tail feather coverts. *J. Exp. Zool. Part Ecol. Genet. Physiol.* **313A**, 690–703.

Williams, C. L., Hagelin, J. C. and Kooyman, G. L. (2015). Hidden keys to survival: the type, density, pattern and functional role of emperor penguin body feathers. *Proc R Soc B* **282**, 20152033.

Wolfe, J., Hill, D. N., Pahlavan, S., Drew, P. J., Kleinfeld, D. and Feldman, D. E. (2008). Texture coding in the rat whisker system: Slip-stick versus differential resonance. *PLOS Biol.* **6**, e215.

Yorzinski, J. L., Patricelli, G. L., Babcock, J. S., Pearson, J. M. and Platt, M. L. (2013). Through their eyes: selective attention in peahens during courtship. *J. Exp. Biol.* **216**, 3035–3046.

Yu, Y. S. W., Graff, M. M. and Hartmann, M. J. Z. (2016). Mechanical responses of rat vibrissae to airflow. *J. Exp. Biol.* **219**, 937–948.

Figure 1

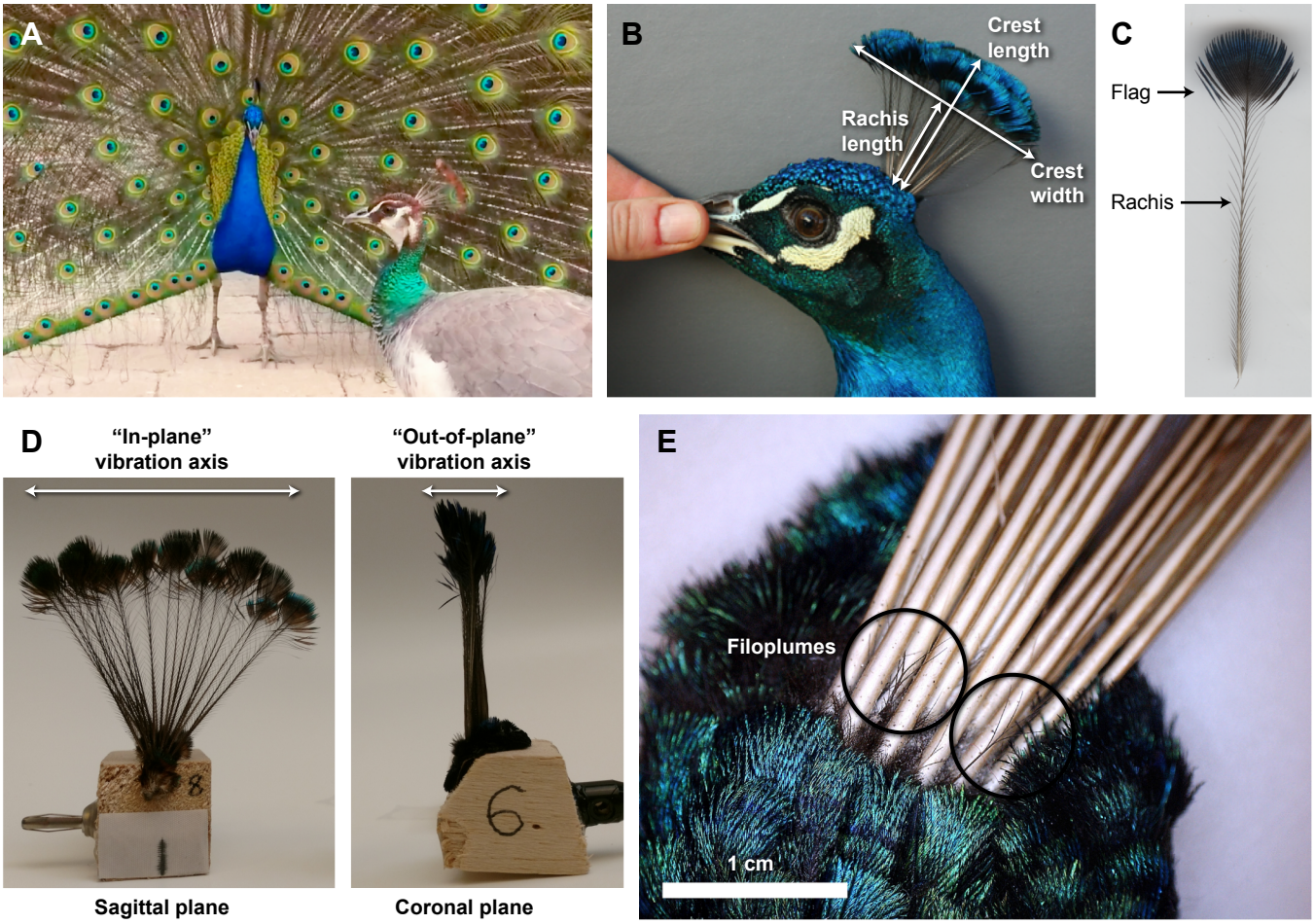
A
B
Crest length
Rachis length
Crest width
C
Flag
Rachis
D
"In-plane" vibration axis
"Out-of-plane" vibration axis
Sagittal plane
Coronal plane
E
Filoplumes
1 cm

Figure 2

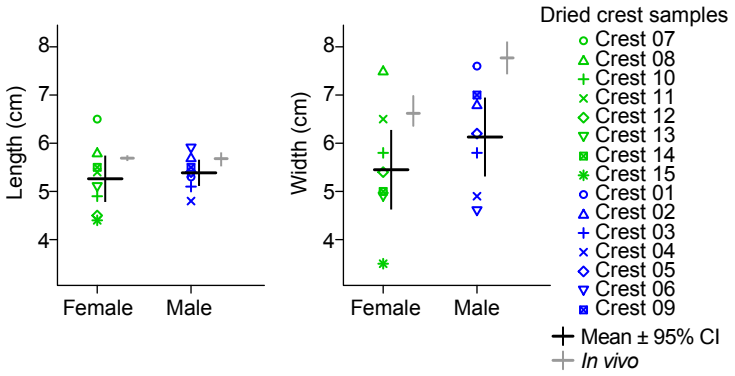
Length (cm)
8
7
6
5
4
Female
Male
Width (cm)
8
7
6
5
4
Female
Male
Dried crest samples
Crest 07
Crest 08
Crest 10
Crest 11
Crest 12
Crest 13
Crest 14
Crest 15
Crest 01
Crest 02
Crest 03
Crest 04
Crest 05
Crest 06
Crest 09
Mean ± 95% CI
In vivo

Figure 3

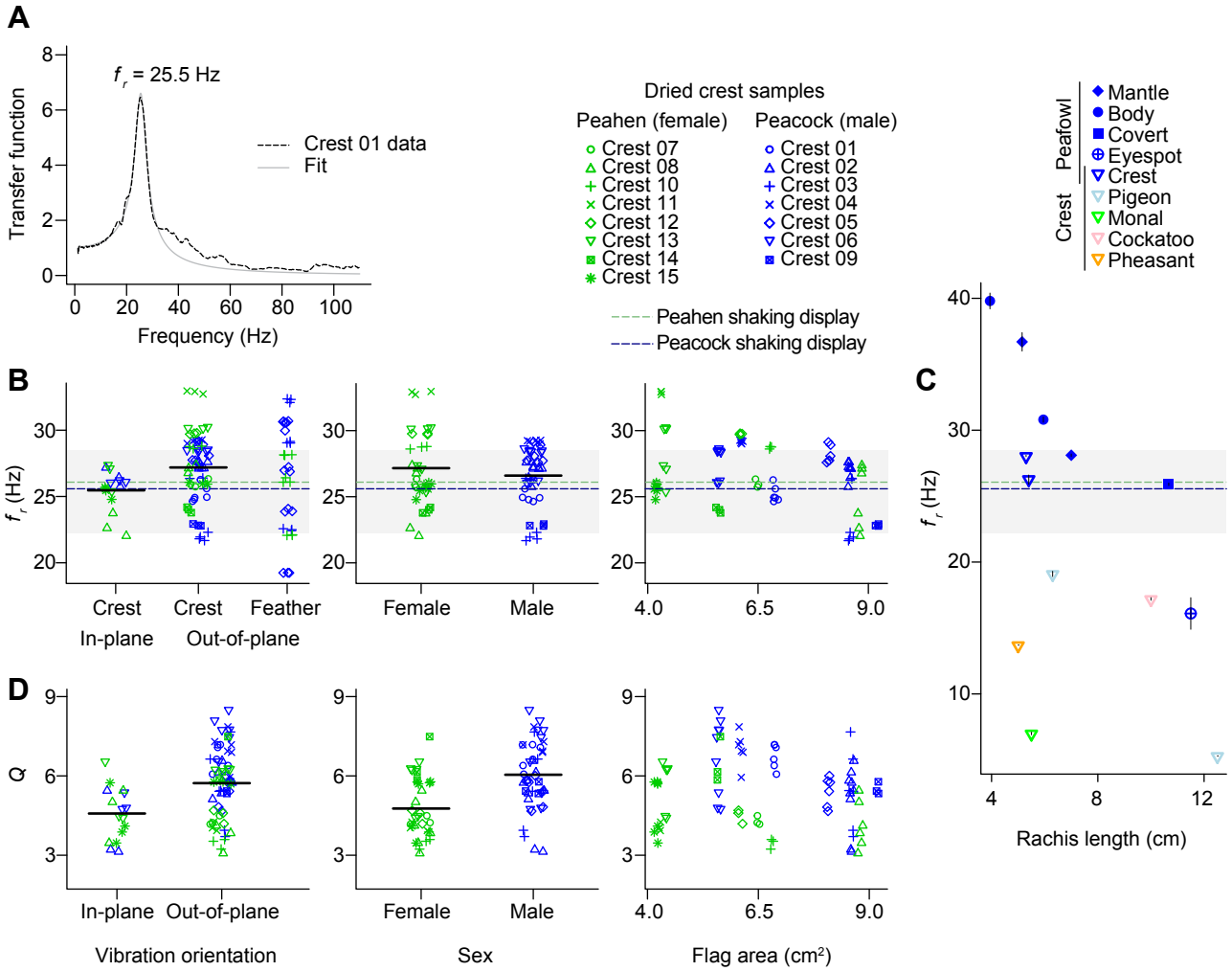
A
f_r = 25.5 Hz
Transfer function
Crest 01 data
Fit
Frequency (Hz)
Dried crest samples
Peahen (female)
Crest 07
Crest 08
Crest 10
Crest 11
Crest 12
Crest 13
Crest 14
Crest 15
Peacock (male)
Crest 01
Crest 02
Crest 03
Crest 04
Crest 05
Crest 06
Crest 09
Peahen shaking display
Peacock shaking display
Peafowl
Mantle
Body
Covert
Eyespot
Crest
Crest
Pigeon
Monal
Cockatoo
Pheasant
B
f_r (Hz)
Crest In-plane
Crest Out-of-plane
Feather
Female
Male
4.0
6.5
9.0
C
f_r (Hz)
Rachis length (cm)
D
Q
In-plane
Out-of-plane
Vibration orientation
Female
Male
Sex
Flag area (cm²)

Figure 4

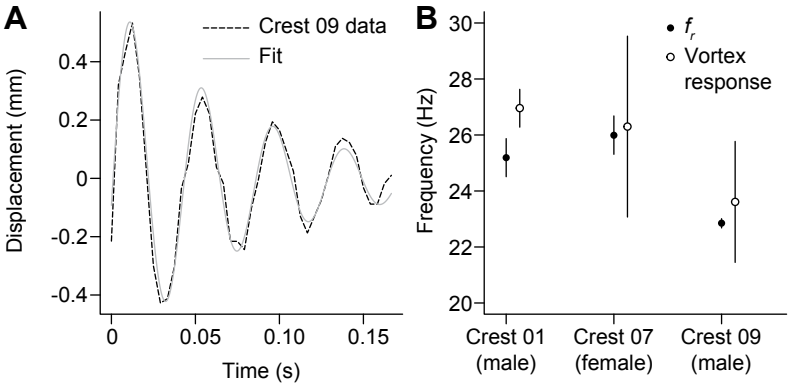
A
Crest 09 data
Fit
Displacement (mm)
0.4
0.2
0
-0.2
-0.4
0
0.05
0.10
0.15
Time (s)
B
f_r
Vortex response
Frequency (Hz)
30
28
26
24
22
20
Crest 01 (male)
Crest 07 (female)
Crest 09 (male)

Figure 5

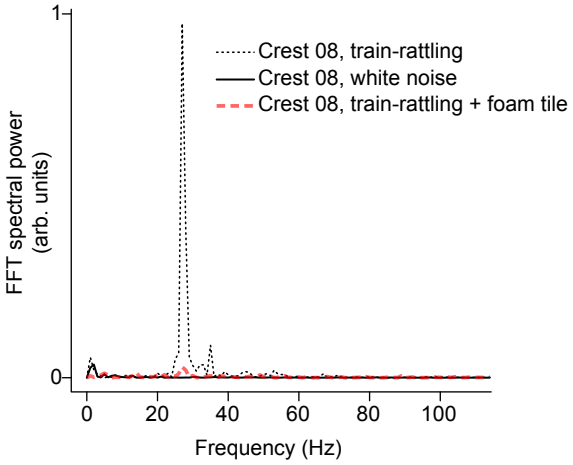
1
0
FFT spectral power
(arb. units)
Crest 08, train-rattling
Crest 08, white noise
Crest 08, train-rattling + foam tile
0
20
40
60
80
100
Frequency (Hz)
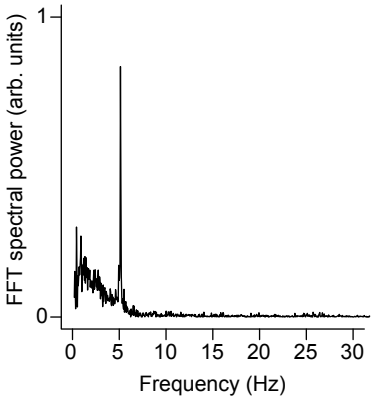
Figure 6